Chemical Physics 116 (1987) 299–309
North-Holland, Amsterdam

A GENERAL PURPOSE XUV LASER SPECTROMETER: SOME APPLICATIONS TO N_2, O_2 AND CO_2

T.P. SOFTLEY [1], W.E. ERNST [2], L.M. TASHIRO and R.N. ZARE

Department of Chemistry, Stanford University, Stanford, CA 94305, USA

Received 27 April 1987

Coherent radiation is generated from 90 to 105 nm by frequency tripling the frequency-doubled output of a pulsed Nd:YAG-pumped dye laser using a synchronized pulsed jet of various gases as the nonlinear medium. The XUV radiation is isolated by a pair of dichroic mirrors before interacting with a supersonically cooled gas target. Provisions have been made to measure the photoion yield as a function of wavelength using a time-of-flight mass spectrometer. In addition absorption by the target gas or fluorescence from the excited target and/or its fragments can be detected. Some applications are presented which illustrate the versatility of this XUV laser spectrometer involving 1+1 resonance-enhanced multiphoton ionization of N_2 and excitation of Rydberg states of O_2 and CO_2.

1. Introduction

Compared to spectroscopic studies at longer wavelengths, the XUV region of the electromagnetic spectrum (wavelengths between 105 nm and soft X-rays) has received little attention. In large part, this has been a consequence of the lack of bright tunable sources. However, the introduction of synchrotron radiation [1] is rapidly altering this field, although such sources require regional or national facilities. Another development of potential importance is the use of nonlinear optics to breach this region of the spectrum because such techniques can be carried out in the laboratory of an individual investigator [2]. This paper describes the construction of a general-purpose XUV spectrometer based on frequency tripling the frequency-doubled output of a pulsed dye laser.

In 1973 Harris and co-workers [3] showed that frequency tripling in phase-matched gas mixtures was a useful method to extend the valuable properties of coherent radiation into the vacuum ultraviolet. Subsequently, sum and difference frequency mixing of the output from two lasers enabled a fairly complete coverage of the VUV range 180–105 nm [4]. A particular limitation of the technique was the necessity to separate the nonlinear medium from the spectroscopic sample cell by a lithium fluoride window whose transmission cutoff is about 105 nm. No other suitable window materials were available to allow extension to shorter wavelengths.

In 1983 Marinero et al. [5] reported generation of continuously tunable coherent XUV radiation (97.3–102.3 nm) by frequency tripling in a pulsed free jet. The jet provided the required high density of gas close to the orifice, while the background pressure remained low. This enabled a windowless differentially pumped chamber to be used. Wallenstein and co-workers [6] have recently demonstrated that tunable coherent radiation at wavelengths as short as 50 nm can be produced via resonantly enhanced fifth harmonic generation in a free jet of argon or neon. In general, the frequency upconversion of pulsed lasers gives VUV or XUV radiation of higher spectral brightness than other radiation sources in this spectral region. In addition, the polarization of the radiation

[1] Harkness Fellow of the Commonwealth Fund; present address: University Chemical Laboratory, Lensfield Road, Cambridge CB2 1EW, UK.

[2] Heisenberg Fellow; present address: Institut für Molekülphysik, Fachbereich Physik, Freie Universität Berlin, Arnimallee 14, D-1000 Berlin 33, Germany.

is easily adjustable and the light source has the convenience of being a laboratory-scale experiment whose costs are modest in comparison to synchrotron radiation sources.

A number of applications of this new light source may be envisaged. The lowest electronically excited states of many atoms and molecules lie in the VUV or XUV regions; thus the availability of a coherent light source in this range not only allows high-resolution spectroscopic studies, but is also valuable for state-selective detection of molecules in dynamical experiments. Photoionization studies of molecules also require short-wavelength radiation. For example, a narrow-bandwidth radiation source would be particularly helpful for study of autoionization structure. In addition, the high brightness of the source may allow observation of low cross-section processes of special interest, such as double excitation events or near-threshold behavior.

2. The XUV spectrometer

2.1. Generation of XUV radiation

Fig. 1 shows schematically the experimental arrangement. A Nd : YAG-pumped dye laser (Quanta Ray DCR-1/PDL-1) with frequency doubler (Wex 1A) provides tunable radiation in the range 330–270 nm using the dyes DCM, R640, kiton red, R610, R590, and fluorescein 548 in methanol. Typical pulse energies of 8–15 mJ in a 6 ns pulse length at a 10 Hz repetition rate are obtained. The UV is focused by a 25 cm quartz lens into the tripling chamber. A pulsed valve (Lasertechnics LPV) is mounted on a three-way translation stage for positional optimization and the 0.5 mm nozzle orifice is located less than 1 mm from the laser focal point. For a theoretical treatment of frequency tripling in pulsed free jets, the reader is referred elsewhere [7]. In the experiments described below we have used argon, krypton or xenon as the tripling gas. In general, xenon provides the best conversion efficiency; at certain wavelengths, however, the generated XUV is significantly absorbed by xenon leading to discontinuities in the tuning curve. In contrast, the power curve of argon is smooth, but the efficiency on average is less than xenon by more than an order of magnitude. A stagnation pressure of 50 psig is normally employed behind the nozzle for all gases and the pulse length is 200 μs. The conversion efficiency for non-resonantly enhanced frequency

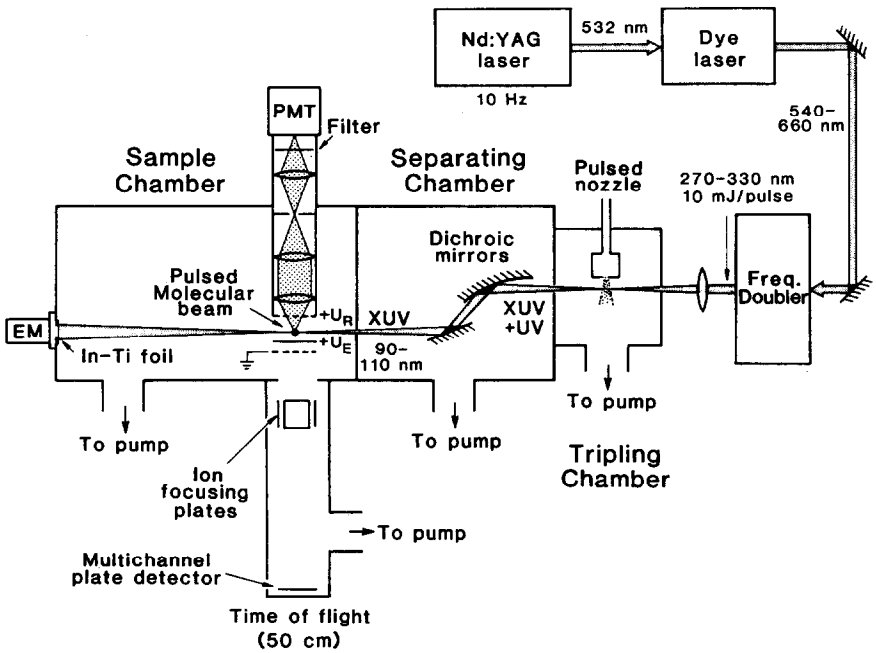

Fig. 1. The XUV laser spectrometer.

tripling is at best 10^{-6} under our experimental conditions. From the measured ionization signal for gases of known cross section we estimate typical XUV powers of 2×10^8 photons per pulse. The spectroscopic bandwidth, determined by the dye laser bandwidth is 1.2 cm^{-1} in the XUV; the dye laser is used without an intracavity etalon.

2.2. The separation chamber

The light exiting the tripling chamber, through a 5 mm aperture, consists mostly of the UV fundamental. For many experiments the vast excess of UV radiation will result in the occurrence of unwanted processes, such as photodissociation or multiphoton ionization of the sample. Separation of the two colors is therefore important. However, for the 90–105 nm region this has proved to be a technical challenge. The only known UV absorbing, XUV transmitting filter materials are thin ($\approx$ 1000 Å) metal foils, such as a 99% In–1% Ti alloy. While these absorb 100% of the UV (attenuation $\approx 10^7$), the best transmission is 5% in the 90–105 nm range and the foils are very susceptible to UV laser damage. An alternative is the use of a dispersive element. In our laboratory we have previously used [5] a vacuum monochromator (Acton Research VM 502) which employs a reflective aluminum diffraction grating overcoated with MgF_2. Again, near-perfect separation is obtained in first order, but the efficiency for XUV is of order 5% Furthermore we have found significant laser damage to the grating after a few hours of operation using a peak UV power density of 5 MW/cm^2.

The experiments described in this paper employed a new separation device based on the work of Falcone and Bokor [8]. The separating chamber consists of two specially designed dichroic mirrors (beam splitters), each of which consists of a quartz substrate overcoated with a single layer of magnesium fluoride (Acton Research). The UV/XUV beams impinge both mirrors at a 70° incidence angle with s-polarization (electric vector perpendicular to the plane of incidence). The XUV reflectivity is about 45% at each optic. The thickness of the MgF_2 layer is such as to provide an antireflective coating for the UV at the 70° incidence angle; thus 99% of the UV radiation is transmitted at λ_{max}. The use of two mirrors, therefore, reduces the reflected UV by four orders of magnitude while 20% of the XUV is reflected into the sample chamber. Although this still leaves an excess of UV in the beam, the probability of nonlinear (multiphoton) processes will be reduced by many more orders of magnitude. A disadvantage of the mirrors is that the UV antireflective coating is necessarily narrowband. The UV reflectivity at each mirror rises to about 5% at $\lambda_{max} \pm 10$ nm.

A general problem of using optical surfaces inside oil-diffusion-pumped vacuum chambers is laser damage to the optics caused by laser-induced polymerization of the oil film on the optics. To overcome this obstacle we use a turbomolecular pump in the chamber housing the dichroic mirrors. We also employ in the oil diffusion pumps elsewhere in the XUV spectrometer a fluorocarbon oil (Fomblin H-Vac 25/9) which is known to resist polymerization [9].

An important additional feature of our separation chamber is that the first mirror has a toroidal geometry in order to refocus the diverging light from the tripling chamber. (A spherical mirror would be highly astigmatic at the 70° incidence angle.) Radii of curvature $R_1 = 100$ cm and $R_2 = 12.5$ cm are used to give a focal length of 17.1 and 18.3 cm in the tangential and sagittal planes, respectively [10,11]. The beam waist at the focal point is about 1 mm and is relatively free from astigmatism. Because no solid lens materials exist in the XUV this arrangement is particularly convenient as it enhances the power density, allowing interaction with small sample volumes.

2.3. The sample chamber

The XUV focal point is located between a pair of ion repeller and extractor plates in a differentially pumped sample chamber. The light is crossed at this point by a pulsed molecular beam of the sample under investigation, originating from a solenoid valve (General Valve series 9). Photoions can be sent through a slit in the extractor plate into a 50 cm time-of-flight mass spectrometer with a multichannel plate detector. Potentials of +1400

and +1100 V are normally applied to the repeller and extractor plates, respectively, to detect positive ions. The sharp focus of the XUV light permits excellent mass resolution in the time-of-flight spectrometer; six isotopes of xenon, masses 129–136 are easily distinguishable for example. The repeller plate consists of an 90% transmitting nickel electroformed mesh. This allows fluorescent light from the sample to be sent via a set of light collecting optics to a photomultiplier located outside the vacuum chamber. The third diagnostic available is an electron multiplier (EMI 9643/2B) mounted behind an In/Ti filter beyond the sample interrogation region. This allows monitoring of the transmitted XUV intensity enabling the measurement of an absorption spectrum.

3. Applications

To date relatively few spectroscopic studies have been performed with coherent VUV or XUV radiation sources [2,12] and only two applications of XUV radiation generated in a free jet have been reported [5,13]. We present here the application of XUV radiation to the spectroscopy of the molecules N_2, O_2 and CO_2. A further study in the same apparatus on the Stark structure of atomic xenon Rydberg states has been described elsewhere [14]. The examples are chosen to illustrate the versatility and practicality of an XUV laser spectrometer. Although each of these studies are in primitive early stages, it is clear that such a device has the potential for greatly extending our knowledge of the behavior of molecules in this difficult region of the electromagnetic spectrum.

3.1. $N_2(b'^1\Pi_u - X^1\Sigma_g^+)$

In fig. 2 we show the (1, 0) vibrational band of the $N_2(b'^1\Pi_u - X^1\Sigma_g^+)$ system. The spectrum was recorded by monitoring the N_2^+ ion yield versus laser wavelength. Figs. 2a and 2b are spectra taken with a jet-cooled molecular beam and a bulk room-temperature sample, respectively. The assignments shown are based on the high-resolution absorption spectrum taken in the second order of a 6 m vacuum spectrograph by Carroll and Collins

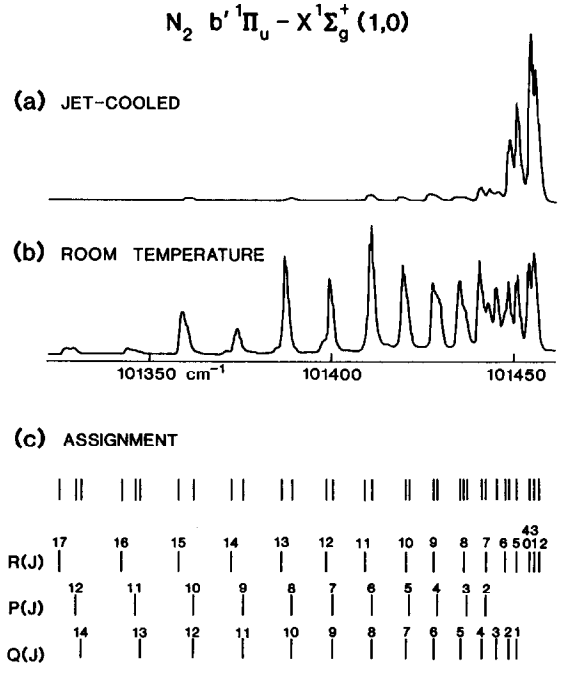

Fig. 2. 1+1 REMPI spectrum of the $N_2(b'^1\Pi_u - X^1\Sigma_g^+)$ (1, 0) band, showing N_2 ion yield versus wavenumber: (a) jet cooled (10 K), (b) room temperature, and (c) spectral assignments (see Caroll and Collins [15]).

[15]. From the intensities of the lines shown in fig. 2a we estimate a rotational temperature of 10 K for the molecular beam. The $b'^1\Pi_u$ state of N_2 lies below the ionization limit (IP = 15.5808 eV [16]). Thus the appearance of N_2^+ ions at resonance requires the absorption of two photons, i.e. a 1 + 1 resonance-enhanced multiphoton ionization (REMPI). We assume that the ionizing photon is from the background UV radiation. However, the resonant photon is certainly of XUV wavelength because no N_2^+ ions can be detected in the absence of XUV, i.e. when the pulsed tripling valve is switched off.

A 1 + 1 REMPI spectrum has not been previously recorded for N_2, although the 2 + 2 REMPI spectrum of the $a^1\Pi_g - X^1\Sigma_g^+(1, 0)$ band has been reported [17,18]. The linewidths shown in fig. 2 are determined by the laser bandwidth (≈ 1.2 cm^{-1}) and in some cases by the overlap of rotational branches. This resolution does not represent any significant improvement over the work of Carroll and Collins [15]. The use of an intracavity

etalon in the dye laser, however, would certainly lead to full resolution of all rotational lines without any loss in sensitivity.

Although no new spectroscopic knowledge has been gained from this study, we believe that this result may be of considerable value in the state-selective detection of N_2 molecules in dynamical experiments [18]. The 1 + 1 REMPI process has the potential advantage of being more sensitive and easier to interpret than the 2 + 2 process. The detection sensitivity at present is of order 10^{10} molecules/cm^3 per quantum state. This limit could be improved considerably by the use of resonantly enhanced sum-frequency mixing of two lasers in the XUV generation process [6]. This N_2 spectrum has been found to be of great value in subsequent experiments described below in that it could be used to quantify the rotational temperature of the jet-cooled molecular beam. It also serves as a convenient calibration spectrum in this region of the XUV.

3.2. Autoionization spectrum of $O_2(H\,^3\Pi_u - X\,^3\Sigma_g^-)$

In 1975 Dehmer and Chupka [19] carried out a detailed study of autoionization structure in the photoionization efficiency curve of O_2. A portion of their spectrum is shown in fig. 3. The light source used was a helium continuum lamp together with a 3 m normal incidence monochromator to give a spectroscopic resolution of 0.015 nm in the range of 94.0–103.0 nm and 0.007 nm below 94 nm. The gas was pre-cooled to 77 K before entering the ionization chamber.

The features in the 94–101 nm region were subsequently reassigned in 1984 by Nishitani et al. [20] to a single vibrational progression of the transition $H\,^3\Pi_u$; $3s\sigma_g - X\,^3\Sigma_g^-$. A second progression beginning at 94 nm was assigned to the transition $J\,^3\Pi_u$; $3s\sigma_g - X\,^3\Sigma_g^-$. No clear rotational structure was observed for any of the bands in either study. It was not established whether this was a result of inadequate spectroscopic resolution, insufficient rotational cooling, or autoionization broadening.

We have re-recorded seven of the vibrational bands at 0.001 nm resolution, under the same conditions of rotational cooling as were used in

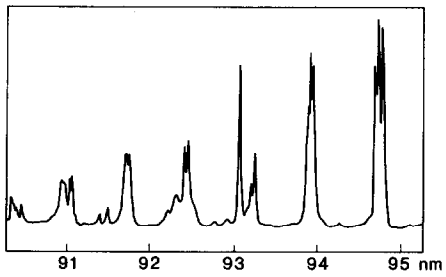

Fig. 3. 77 K photoionization efficiency spectrum of O_2 at 0.007 nm resolution (taken from Dehmer and Chupka [19]).

taking the N_2 spectrum, i.e. about 10 K. In this case the upper levels of the transitions lie above the ionization limit (IP of $O_2 = 12.071$ eV [16]). Thus the O_2^+ ions can be detected at resonance via the absorption of just one XUV photon followed by autoionization. We find that negligible photoionization of O_2 occurs when the XUV is removed, i.e. there is no off-resonant multiphoton ionization caused by the remnant UV. The effects of rotational cooling are shown in fig. 4 where we compare jet-cooled and room-temperature spectra for one band. Fig. 5 shows all seven bands. The spectra are uncorrected for XUV intensity variations; hence fig. 5 does not necessarily represent true relative intensities. In most cases new struc-

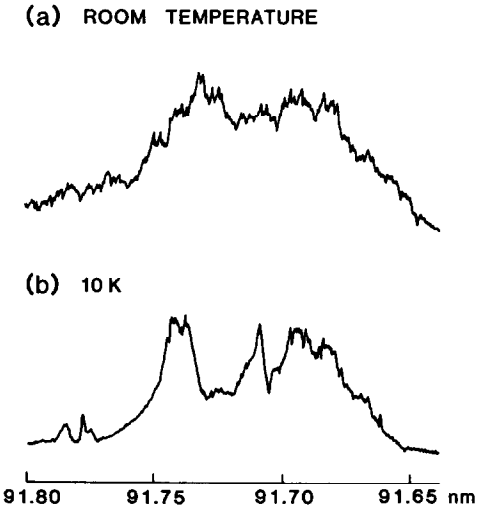

Fig. 4. Effects of rotational cooling on the autoionization band of O_2 at 91.7 nm: (a) room temperature and (b) jet cooled (10 K).

ture is seen compared to the work of Dehmer and Chupka [19] (see fig. 3). For example, the band at 91.7 nm shows several distinct features in our spectrum while only appearing as two features in the spectrum of Dehmer and Chupka. Disappointingly, no clearly resolved rotational structure is seen in our spectrum. The ground-state rotational constant [16] is known to be 1.446 cm^{-1} for O_2 and it would seem likely that our spectroscopic resolution would be sufficient to observe rotational structure. We therefore conclude that the spectrum is subject to autoionization broadening. Autoionization linewidths of 5 cm^{-1} would correspond to lifetimes of about 1 ps. At present we have been unable to account for the observed structure in the individual bands, although we suspect that this is a consequence of the rotational branch structure associated with a $^3\Pi$–$^3\Sigma$ transition.

3.3. Rydberg series of CO_2

In this section we report a study of the photodissociation of CO_2, in which the total production of fluorescence from the process

$$CO_2 + h\nu \rightarrow CO(a'\,^3\Sigma^+, d\,^3\Delta_i, e\,^3\Sigma^-) + O(^3P)$$
$$\downarrow$$
$$CO(a^3\Pi) + h\nu'$$

was measured as a function of photodissociation wavelength, 90.3–92.5 nm.

The red fluorescence was separated from the background radiation using a long-wavelength-pass cutoff filter (Corion LL-600R) and sent to a red-sensitive photomultiplier (RCA C31034). The fluorescence lifetime is a few microseconds; thus the fluorescence can also be separated from the 6 ns laser pulse using a boxcar averager. For comparison we have recorded an absorption spectrum in the same spectroscopic region and also a REMPI spectrum; this example therefore makes use of all three possible diagnostics available to our XUV laser spectrometer. The spectra are shown in fig. 6; all three were recorded at 0.001 nm resolution. The absorption spectrum (fig. 6a) was obtained by monitoring the transmitted XUV signal at the electron multiplier and is uncorrected for XUV variation across the dye curve (Fluorescein 548), i.e. the figure has a curved baseline. The density of molecules at a 5 mm distance from the nozzle was sufficient to produce nearly 50% absorption at resonance.

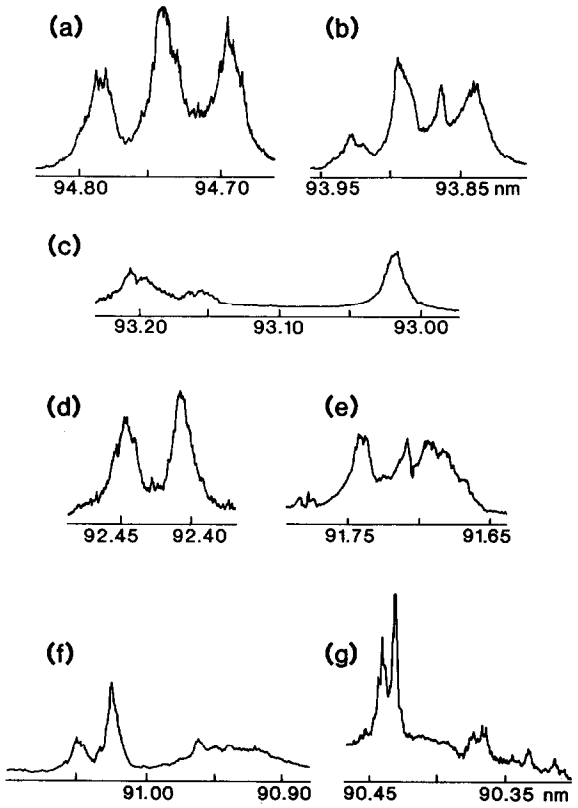

Fig. 5. Seven bands of the jet-cooled autoionization spectrum of O_2 at 0.001 nm resolution.

The absorption and photofragment fluorescence–excitation spectra are very similar, each showing the same resonance features with approximately the same relative intensities. However, careful examination of the spectra reveals that at the long-wavelength side where the absorption features are not overlapped, the peak height to valley ratio is about 3 : 1 for the fluorescence excitation while it is only 2 : 1 for absorption. Obviously there is a broadband continuous absorption underlying the resonance features of the absorption spectrum which makes a smaller contribution to the production of the fluorescing triplet states of CO.

The VUV/XUV absorption and photodissocia-

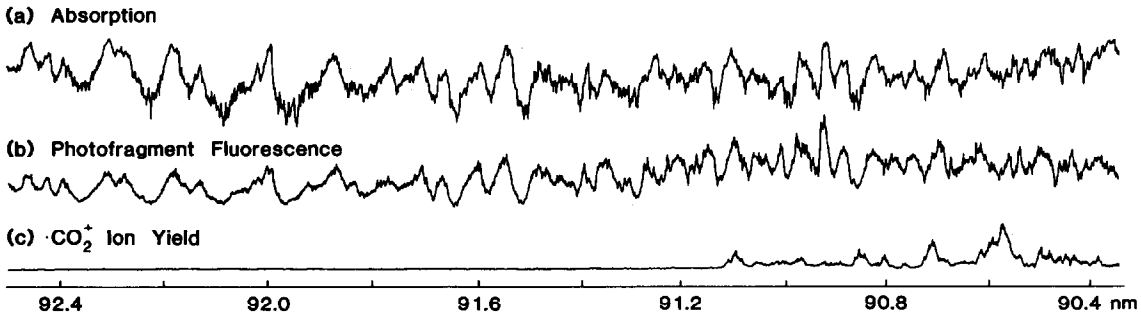

Fig. 6. Absorption, photofragment fluorescence excitation and CO_2^+ photoion yield spectra for the region 92.5–90.3 nm. The spectra are uncorrected for variations in dye-laser efficiency (see text).

tion of CO_2 has been the subject of considerable interest previously. The Rydberg states of CO_2 leading to the first ionization limit (89.99 nm) were first classified by Price and Simpson [21] in 1938. Tanaka, Jursa and LeBlanc [22] subsequently recorded the absorption spectrum at higher resolution, and were able to extend the series obtained by the former workers to higher principal quantum number. Absolute absorption cross sections were measured through this region by Nakata et al. [23] and by Cook et al. [24], both at 0.02 nm resolution. In the 90.3–92.5 nm range these absorption cross sections represent the sum of as many as nine photodissociation channels (see table 1). Channels 7 through 9 are only possible for a part of this range. Our photofragment fluorescence measurements correspond to channels 5 through 7.

The photodissociation through these three channels was previously studied by Judge and Lee [27] who used an atomic nitrogen emission lamp as the light source. Only a single wavelength (92.3 nm) was available to them in the range studied here however. They measured a cross section for triplet fluorescence production of 25 Mb, which was approximately half the total absorption cross section at this wavelength. Phillips, Lee and Judge [28] also studied photodissociation through the spin-forbidden channel 9 at the same wavelength obtaining a much smaller cross section for production of VUV fluorescence ($CO(A^1\Pi \rightarrow X^1\Sigma^+)$).

Lawrence [29] used a combination of a continuum lamp and a monochromator as a tunable XUV source (resolution 0.1 nm) for the excitation of CO_2 in the range 109–85 nm and detected $CO(a^3\Pi–X^1\Sigma^+)$ UV phosphorescence from the fragments. In this way he monitored the sum of direct production of $a^3\Pi$ (channels 4 and 8) and also production of all higher triplet states (channels 5–7) which cascaded into the $a^3\Pi$ state. Lawrence found the same features in the phosphorescence spectrum as in the total cross section measurements of Nakata et al. [23]. In contrast to our findings, however, he concluded that there was no significant difference in the peak height to valley ratios between the absorption and the phosphorescence–excitation spectra. The fraction of the total dissociation occurring through channels 4 through 8 showed a gradual smooth increase across the measured range reaching a value of about 50% of 92 nm. The fraction did not depend on whether the photodissociation wavelength was on- or off-resonance.

Lawrence discussed his observations with reference to some previous molecular orbital calcula-

Table 1
CO_2 photofragmentation channels

Channel number	Process	Threshold [a] (nm)
1	$CO_2 \rightarrow CO(X^1\Sigma^+)+O(^3P)$	227.4
2	$CO_2 \rightarrow CO(X^1\Sigma^+)+O(^1D)$	167.1
3	$CO_2 \rightarrow CO(X^1\Sigma^+)+O(^1S)$	128.6
4	$CO_2 \rightarrow CO(a^3\Pi)+O(^3P)$	107.9
5	$CO_2 \rightarrow CO(a'^3\Sigma^+)+O(^3P)$	100.2
6	$CO_2 \rightarrow CO(d^3\Delta_i)+O(^3P)$	95.1
7	$CO_2 \rightarrow CO(e^3\Sigma^-)+O(^3P)$	92.4
8	$CO_2 \rightarrow CO(a^3\Pi)+O(^1D)$	92.1
9	$CO_2 \rightarrow CO(A^1\Pi)+O(^3P)$	91.7

[a] Calculated from refs. [16,25,26].

tions and electron energy loss measurements of Krauss et al. [30]. The continuum-like absorption underlying the spectrum was attributed to a repulsive $^1\Sigma_u^+$ valence state. The Rydberg states were predissociated by this interloper valence state, the curve crossing taking place outside the Franck–Condon region. Having crossed to the repulsive surface, the molecules lose memory of the original excitation; hence the branching ratios are the same for direct dissociation or for predissociation.

Our measurements appear to contradict this conclusion, in that they show that the branching ratio is not constant. The difference between our observations and those of Lawrence may arise because we do not monitor the direct population of CO($a\,^3\Pi$) (channels 4 and 8); it is possible that the probability ratio of channels 4 and 8 to channels 5 through 7 is wavelength dependent, while the sum of all five channels is wavelength independent as found by Lawrence. A more likely explanation for the difference lies in our 100-times better resolution. Features separated by less than 100 cm^{-1} would be overlapped in the spectrum of Lawrence and it is probable that there would be no truly off-resonant regions in the range 92.5–90.3 nm at this resolution. Under these circumstances the peak to valley contrast would be somewhat reduced. In summary, although the conclusion of Lawrence and of Krauss may be essentially correct, our better resolution allows us to raise the possibility that the single-perturbing state model may be an oversimplification.

We have also measured the polarization of the fluorescence excitation spectrum with respect to the laser polarization. We find no measurable difference for the spectra polarized in the parallel or perpendicular directions relative to the electric field vector of the XUV; taking our signal to noise into account, we conclude that the polarization is less than 5%. This result is not surprising, given that both the excitation of the parent molecule and the fluorescence are not rotationally resolved; hence the polarization from various branches averages close to zero.

The absorption and photofragment-fluorescence spectra show all the resonance features originally reported by Tanaka et al. [22] and a number of other features too. Tanaka identified four series converging to the lowest ionization limit $CO_2^+(\tilde{X}^2\Pi_g)$, three of which lead to the $J = 3/2$ spin–orbit component with average quantum defects $\delta = -0.35$, -0.43 and -0.03, while one series leads to the $J = 1/2$ component, $\delta = -0.35$. In 1969 Lindholm [31] discussed the assignment of these series together with those converging to higher electronic states of the ion. By comparison with analogous series in other small molecules he concluded that the quantum defects should be positive, listing values of $\delta = 0.7$, 0.57 and 0.0. This change led to a renumbering of the principal quantum numbers of the first two series. Fridh, Åsbrink and Lindholm [32] subsequently identified the orbital characteristics of these series as $np\sigma_u$, $np\pi_u$ and nf_u, respectively, by performing semi-empirical MO calculations.

Recently Cossart-Magos et al. [33] have remeasured the absorption spectrum of CO_2 in a 10 m VUV spectrograph at 0.0008 nm resolution over the range 114–89 nm. They clearly identified the nf Rydberg series leading to the $CO_2^+(\tilde{X}^2\Pi_g)$ $J = 1/2$ limit up to $n = 32$ and the $\tilde{X}^2\Pi_g$ $J = 1/2$ limit up to $n = 28$. These workers were thus able to obtain very accurate values for the two ionization limits of 111121 ± 2 and 111281 ± 2 cm^{-1}, respectively. It is not easy to compare our absorption spectrum with the photographic recording of Cossart-Margos et al. as they did not obtain a densitometer trace, and their spectrum was recorded at room temperature whereas ours was jet cooled. Nevertheless we have used their experimentally determined ionization limits to calculate the effective quantum numbers at the energies corresponding to the absorption maxima in fig. 6a. On this basis we grouped the features into two sets of three series converging to the two spin–orbit components of the lowest ionization limit, as shown in table 2. The average quantum defects are in good agreement with those given by Lindholm. The assignment of specific absorption features should be considered tentative because of the diffusive nature of the bands and the high density of states in this spectroscopic region. According to the work of Cossart-Magos et al. [33] the ordering of the $np\sigma_u$ and $np\pi_u$ series must be reversed with respect to ref. [32], assigning the larger quantum defect to the $np\pi_u$ series.

Fig. 6c shows the CO_2^+ ion production for this spectroscopic region. Once again the spectrum does not appear when the pulsed tripling nozzle is switched off, demonstrating that at least one XUV photon is required to produce each CO_2^+ ion. In fact a second photon is also required for ionization because the ionization limit of CO_2 lies at shorter wavelength than the region under study. The lowering of the ionization potential by the electric field used for extracting the ions is less than 50 cm^{-1} under our experimental conditions; thus field-induced ionization cannot be important here. It can be seen from fig. 6c that there are no resonances or background signal in the range 92.5–91.1 nm while those features which do appear to shorter wavelength do not correspond to those seen in absorption. It is apparent that the Rydberg states converging on the first ionization limit do not act as resonant intermediate states in the two-photon ionization spectrum. Furthermore, the absence of the observed REMPI features in the absorption spectrum suggests that the prob-

Table 2
Bandheads observed in the photofragment fluorescence excitation spectrum (fig. 6b)

n	1A		2A		3A	
	wavenumber	n^*	wavenumber	n^*	wavenumber	n^*
series converging to $CO_2^+(\tilde{X}^2\Pi_{g3/2})$; limit = 111121 cm^{-1}						
7	108856.6	6.96	108310.2 108344.2	6.25 6.29	108457.0	6.42 [a]
8	109384.7	7.95	109060.9	7.30	109138.5	7.44
9	109781.4	9.05	109486.3	8.19	109581.5	8.44
10	109992.1	9.86 [a]	109844.8	9.27	109883.3	9.42
11	110217.3	11.02	110060.1	10.17 [a]	110117.1	10.45
12	110363.7	12.04 [a]	110247.0	11.21 [a]	110285.9	11.46 [a]
13	110451.8	12.81 [a]	110384.3	12.20	110408.3	12.41 [a]
14	110568.9	14.10 [a]	110503.6	13.33 [a]		
δ		0.003		0.75		0.57
series converging to $CO_2^+(\tilde{X}^2\Pi_{g1/2})$; limit = 111281 cm^{-1}						
6	108170.7 108205.5	5.94 5.97	–		–	
7	109013.2 [a]	6.96	108457.0 108512.8	6.23 [a] 6.30	108662.2	6.47
8	109533.8	7.93	109204.1	7.27	109278.4 109333.4	7.40 7.51
9	109947.9	9.07	109676.7	8.27	109706.2	8.35
10	110155.8	9.88	109992.1	9.23 [a]	110060.1	9.48 [a]
11	110363.7	10.94 [a]	110247.0	10.30 [a]	110285.9	10.50 [a]
12	110503.6	11.88 [a]	110408.3	11.21 [a]	110451.8	11.50 [a]
13	–		–		110568.9	12.41 [a]
δ		0.05		0.74		0.55

unassigned bandheads [b]

wavenumber	n^*(A)	n^*(B)	wavenumber	n^*(A)	n^*(B)
108127.4	6.05	5.90	109606.3	8.51	8.09
108755.6	6.81	6.59	109642.2	8.62	8.19
108818.6	6.90	6.68	109812.0	9.16	8.64
108932.4	7.08	6.84	110535.6	13.69	12.13
109434.3	8.07	7.71	110606.9	14.61	12.76

[a] Bandheads are assigned to members of two different series.
[b] n^*(A) and n^*(B) are effective quantum numbers with respect to the $CO_2^+(\tilde{X}^2\Pi_{g3/2})$ and $CO_2^+(\tilde{X}^2\Pi_{g1/2})$ ionization limits respectively.

ability of excitation to these resonant intermediate states is at least an order of magnitude weaker than the probability for those states actually observed in absorption.

Tanaka and Ogawa [34] observed Rydberg series converging to higher ionization limits of CO_2; the $CO_2^+(\tilde{A}^2\Pi_u)$ state (Tanaka–Ogawa series) and the $CO_2^+(\tilde{B}^2\Sigma_u^+)$ state (Henning series). We suggest here that the observed features in the REMPI spectrum are the lowest members ($n = 3$) of one or both of these series; the $n = 3$ members have not been identified previously in absorption due to spectral congestion. From the revised assignment table of Fridh et al. [32], the most likely candidate would be the $\tilde{A}^2\Pi_u$–$3s\sigma_g$, $v = 0$ state predicted to lie at 13.5 eV (91.8 nm). A fairly low cross section for excitation to this state would be expected because the Franck–Condon factors for higher members of this Rydberg series are a maximum for $v = 3$ rather than $v = 0$.

At the wavelength of the strongest feature in the REMPI spectrum, the sum of the XUV and the fundamental VUV photon energies (147200 cm^{-1}) is sufficient to produce the $\tilde{A}^2\Pi_u$ state of CO_2^+ in vibrational states up to $v = 6$ or the $\tilde{B}^2\Sigma_u^+$ state in $v = 0$. If the intermediate resonant state is a member of the Tanaka–Ogawa series, then we would expect that ionization would lead to the $\tilde{A}^2\Pi_u$ state of the ion (as the other possible ion states could only be reached by a simultaneous excitation (or de-excitation) of two electrons – a process of low probability). Our hypothesis concerning the nature of the intermediate state could then be proven by detecting $\tilde{A}$–$\tilde{X}$ fluorescence from the ion at resonance. Unfortunately the wavelength of this fluorescence falls close to the UV fundamental laser wavelength making fluorescence detection difficult. Based on calculations, Cossart-Magos et al. [33] do not agree with the assignment of ref. [32] for the $3s\sigma_g$ state of the Tanaka–Ogawa series. This would complicate the interpretation of our observations, particularly regarding the appearance of the threshold for ion production. Clearly more work is needed before we can fully understand the complex nature of the CO_2 Rydberg states.

In summary we have shown several applications of our XUV spectrometer in which the high resolution and tunability of laser sources can help to gain more insight into the structure and dynamics of molecular systems.

Acknowledgement

We thank Dr. Claudina Cossart-Magos for making available to us a preprint of ref. [33]. The financial support of the Navy under contract N00014-87-K-0265 and the National Science Foundation under contract NSF PHY 85-06668 is gratefully acknowledged.

References

[1] E.E. Koch, ed., Handbook on synchrotron radiation (North-Holland, Amsterdam, 1983).
[2] S.E. Harris and T.B. Lucatorto, eds., Laser techniques in the extreme ultraviolet, AIP Conference Proceedings, Vol. 119 (1984).
[3] A.H. Kung, J.F. Young and S.E. Harris, Appl. Phys. Letters 22 (1973) 301.
[4] C.R. Vidal, in: Tunable lasers, eds. I.F. Mollenauer and J.C. White (Springer, Berlin, 1986).
[5] E.E. Marinero, C.T. Rettner, R.N. Zare and A.H. Kung, Chem. Phys. Letters 95 (1983) 486.
[6] R. Hilbig, G. Hilber, A. Lago, B. Wolff and R. Wallenstein, in: Short wavelength radiation: generation and applications, eds. D.T. Attwood and J. Bokor, AIP Conference Proceedings, Vol. 147 (1986) p. 382.
[7] C.T. Rettner, E.E. Marinero, R.N. Zare and A.H. Kung, J. Phys. Chem. 88 (1984) 4459;
A.H. Kung, N.A. Gershenfeld, C.T. Rettner, D.S. Bethune, E.E. Marinero and R.N. Zare, in: Laser techniques in the extreme ultraviolet, eds. S.E. Harris and T.B. Lucatorto (American Institute of Physics, Boulder, 1984) pp. 10–22.
[8] R.W. Falcone and J. Bokor, Opt. Letters 8 (1983) 21.
[9] A.H. Kung, private communication (1986).
[10] P. Kirkpatrick and A.V. Baez, J. Opt. Soc. Am. 38 (1948) 766.
[11] G.A. Massey and A.E. Siegman, Appl. Optics 8 (1969) 975.
[12] K.D. Bonin, T.J. McIlrath and K. Yoshino, J. Opt. Soc. Am. B 2 (1985) 1275.
[13] A.H. Kung, R.H. Page, R.J. Larkin, Y.R. Shen and Y.T. Lee, Phys. Rev. Letters 56 (1986) 328.
[14] W.E. Ernst, T.P. Softley and R.N. Zare, in preparation.
[15] P.K. Carroll and C.P. Collins, Can. J. Phys. 47 (1969) 563.
[16] K.P. Huber and G. Herzberg, Molecular spectra and molecular structure, Vol. 4. Constants of diatomic molecules (Van Nostrand, Princeton, 1979).

[17] K.L. Carleton, K.H. Welge and S.R. Leone, Chem. Phys. Letters 115 (1985) 492.
[18] G.O. Sitz, A.C. Kummel and R.N. Zare, J. Vac. Sci. Technol. A 5 (1987) 513.
[19] P.M. Dehmer and W.A. Chupka, J. Chem. Phys. 62 (1975) 4525.
[20] E. Nishitani, I. Tanaka, K. Tanaka, T. Kato and I. Koyano, J. Chem. Phys. 81 (1984) 3429.
[21] W.C. Price and D.M. Simpson, Proc. Roy. Soc. A 169 (1938) 501.
[22] Y. Tanaka, A.S. Jursa and F.J. LeBlanc, J. Chem. Phys. 32 (1960) 1199.
[23] R.C. Nakata, K. Watanabe and F.M. Matsunaga, Sci. Light 14 (1965) 54.
[24] G.R. Cook, P.H. Metzger and M. Ogawa, J. Chem. Phys. 44 (1966) 2935.
[25] C.E. Moore, Atomic energy levels, Vol. 1, NBS Circular 467 (1948) 45.
[26] G. Herzberg, Molecular spectra and molecular structure, Vol. 3. Electronic spectra and electronic structure of polyatomic molecules (Van Nostrand, Princeton, 1966).
[27] D.L. Judge and L.C. Lee, J. Chem Phys. 58 (1973) 104.
[28] E. Phillips, L.C. Lee and D.L. Judge, J. Chem. Phys 68 (1977) 3688.
[29] G.M. Lawrence, J. Chem. Phys. 56 (1972) 3435.
[30] M. Krauss, S.R. Mielczarek, D. Neumann and C.E. Kuyatt, J. Geophys. Res. 76 (1971) 3733.
[31] E. Lindholm, Arkiv. Fysik 40 (1969) 125.
[32] C. Fridh, L. Åsbrink and E. Lindholm, Chem. Phys. 27 (1978) 169.
[33] C. Cossart-Magos, M. Jungen and F. Launay, Mol. Phys, to be published.
[34] Y. Tanaka and M. Ogawa, Can. J. Phys. 40 (1962) 879.